A Finite Difference Element Method for thin elastic Shells

Daniel Choï

A Finite Difference Element Method for thin elastic Shells

Daniel Choï[a]

[a]*Laboratoire de Mathématiques Nicolas Oresme ,*
Université de Caen
14032 Caen, France

Abstract

We present, in this paper, a four nodes quadrangular shell element (FDEM4) based on a Finite Difference Element Method procedure that we introduce. Its stability and robustness with respect to shear locking and membrane locking problems is discussed. Numerical tests including inhibited and non-inhibited cases of thin linear shells are presented and compared with widely used DKT and MITC4 elements.

Key words: Finite Element Method, Membrane Locking, Shear Locking, Elastic shell, Galekin Method, Finite Difference

1. Introduction

The Finite Element Method based on polynomial interpolation is widely and successfully used in engineering applications. Among major problems encountered in Finite Element Methods is the numerical locking. Classical examples are incompressible continuum, shear locking in beam and plates element and shear and membrane locking in thin shells computation [3, 11, 16, 24, 29]. These locking phenomenon has in common the inability of the (polynomial) shape functions to perform some constraints of the problem (such as incompressibility condition displacements or bendings in case of shell).

The finite element computations of thin elastic shells remains an active research topic and of utmost interest for engineering analysis. The main difficulty in shells computations is the extreme variety of asymptotic behaviors depending on the geometry, boundary conditions and external loading : a perfect shell element must be *locking free* for bending dominated behaviors and in the same time be effective in membrane dominated and mixed behaviors [11].

Various finite element methods claims successful with regard to the locking problems [2, 7, 4, 3, 12, 22], such as Partial Reduced Selective Integration method, Mixed Interpolation method, Discrete Strain Gap method and more recently Smoothed finite element method, [22]. In [14], the shape functions has been identified as closely related to numerical locking for conformal finite elements. For that reason, we wanted to explore the possibility to implement a finite element procedure without shape functions as an alternative. Based on this idea, we define, in this paper, a *Finite Difference Element Method* concept and we present a very simple four nodes quadrangular Finite Difference Element procedure (FDEM4) for thin elastic shell problems, based on Naghdi's model.

The paper is organized as follows, first, we present the Finite Difference Element Method concept and we illustrate with a simple scalar Poisson problem.

The Nagdhi's model of thin elastic shells [6] is exposed in section 3. The FDEM4 shell element is based on this model, it is presented in section 4. The section 5 is devoted to numerical results. The robustness with respect to both shear locking and membrane locking, with regular and distorted meshes is tested. FDEM4's performance is compared with MITC4 and triangular DKT. In accordance with the asymptotic analysis of thin elastic shells, [27, 10, 11], inhibited and non-inhibited cases of shells are treated. In non-inhibited cases, the computed solutions are compared with the solution of asymptotic bending problem [15].

We then conclude and discuss the perspectives of the Finite Difference Element method for thin shell computations and more.

Notations and conventions

In this paper, we employ the Einstein convention of summation on repeated upper or lower indices. The Greek (resp. Latin) indices range over $\{1,2\}$ (resp. $\{1,2,3\}$). The partial derivatives with respect to variables x_α are denoted in lower indices preceded by a comma. The ∇ symbol represents the gradient of one function. We use overarrow to indicate space vectors. The variables x_1, x_2 (resp. x_1, x_2, x_3) live in bounded domain $\Omega \subset \mathbb{R}^2$ (resp. $\mathbb{R}^3$). The Hilbert functional space V will denote a Sobolev space and therefore injects continuously into $H = \mathbb{L}^2(\Omega)$. The Harpoon symbol $\longrightharpoonup$ will indicate a convergence in the weak sense. The O and o symbols represent negligible quantities in the sense that

$$\lim_{h\to 0} O(h) = 0 \quad \text{and} \quad \lim_{h\to 0} \frac{o(h)}{h} = 0.$$

2. Towards a Galerkin Method without shape functions

How to avoid shape functions and in the same time apply a Galerkin method ? To this paradoxical question, one answer we found is the finite difference element method : we simply propose to replace the differential operators by finite difference

approximations in some Galerkin projection procedure. More precisely, we replace the differential expressions of undefined shape functions, involved in the variational form problem by some finite difference approximations at the nodes of integration schemes. Although such idea is not new, the method we propose is very similar to the finite difference energy method [3, 9, 23], we give here a different point of view where the finite difference element method is interpreted as a Galerkin method.

A scalar problem example

For sake of simplicity, we shall present the finite difference element method on a scalar problem (corresponding mathematically to a heat or a membrane problem) over $\Omega \subset \mathbb{R}^2$:

$$\begin{cases} \text{Find } u \in V \text{ such that} \\ \displaystyle\int_\Omega \nabla u.\nabla u^* = \int_\Omega f u^* \quad \forall u^* \in V, \end{cases} \tag{1}$$

where V is the Sobolev space $H_0^1(\Omega)$. The variational problem (1) is the standard Poisson problem with Dirichlet boundary conditions.

Shape functions

Actually, we still need shape functions, at least from a theoretical point of view. The only difference with standard finite element method is that, using finite difference approximations, the explicit form or expression of shape functions need not be explicit.

Let V_h be a subspace of V, generated by a set of shape functions ϕ_i piecewise defined on Ω_h, continuous in Ω, where h denotes the mean size of the elements Ω_i. We can impose some natural conditions :

$$\begin{cases} \phi_i(N_j) = \delta_{i,j}, \\ \quad \phi_i = 0, \quad \text{on } \Omega_k \text{ if } N_i \notin \Omega_k. \end{cases} \tag{2}$$

We have then the decomposition :

$$u_h = u_i \phi_i,$$

where the coefficients u_i will represent the value of u at nodes N_i. We don't impose *a priori* shape functions to realize a partition of unity, but an approximate partition of unity. At this point, we need not to be definitive.

Classically, as $h \to 0$, the subspaces V_h define a set of discrete conformal approximations of V : for any $u \in V$, it is easy to construct a sequence $u_n \in V_h$ such that u_n converge almost everywhere towards u in Ω. Let's consider now u_h, the Galerkin projection of the solution u of (1) in V_h :

$$\begin{cases} \text{Find } u_h \in V_h \text{ such that} \\ \displaystyle\int_\Omega \nabla u_h.\nabla u^* = \int_\Omega f u^* \quad \forall u^* \in V_h \end{cases} \tag{3}$$

It classically reduces to a linear system with the 'stiffness' matrix K :

$$K\hat{u} = L,$$

where

$$\hat{u} = [u_1, \dots u_n]^\top,$$
$$L = [l_1, \dots l_n]^\top,$$

and with

$$K_{ij} = \int_\Omega \nabla\phi_i.\nabla\phi_j \tag{4}$$

$$l_j = \int_\Omega f\phi_j. \tag{5}$$

In classical finite element method, the computation of (4) need the explicit expression of the shape functions on the nodes of integration scheme. Here, the Finite Difference Element Method consists simply in integrating over nodes where we replace differential expressions by some consistent finite difference approximations :

Finite difference approximations over a 4 nodes quadrangle

If we consider a quadrangle defined by N_1, N_2, N_3, N_4, of coordinates (x_i, y_i), and with N_0 as the intersection of the two diagonals, see Figure 1.

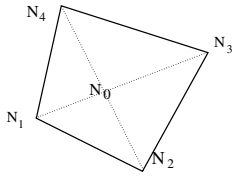

Figure 1: A four nodes quadrangle

By definition, we have, for j = 1,2,3,4 :

$$u(N_j) = u(N_0) + (\nabla u(N_0), \overrightarrow{N_0N_j}) + O(\overrightarrow{N_0N_j}).$$

This gives :

$$\begin{aligned} u(N_3) - u(N_1) &= (\nabla u(N_0), \overrightarrow{N_1N_3}) + O(\overrightarrow{N_0N_3}) - O(\overrightarrow{N_0N_1}), \\ u(N_4) - u(N_2) &= (\nabla u(N_0), \overrightarrow{N_2N_4}) + O(\overrightarrow{N_0N_4}) - O(\overrightarrow{N_0N_2}). \end{aligned} \tag{6}$$

We can then solve the linear system (6) to obtain the *consistent* finite difference central approximation :

$$\nabla u(N_0) = B \begin{bmatrix} u_1 \\ u_2 \\ u_3 \\ u_4 \end{bmatrix} + \max_j(O(\overrightarrow{N_0N_j})), \tag{7}$$

with

$$B = \frac{1}{\Delta} \begin{bmatrix} y_2 - y_4 & y_3 - y_1 & y_4 - y_2 & y_1 - y_3 \\ x_4 - x_2 & x_1 - x_3 & x_2 - x_4 & x_3 - x_1 \end{bmatrix}$$

and

$$\Delta = (x_3 - x_1)(y_4 - y_2) - (x_4 - x_2)(y_3 - y_1).$$

Similarly, it is also possible to write the finite difference on each nodes N_k instead of N_O, for instance :

$$u(N_2) = u(N_1) + (\nabla u(N_1), \overrightarrow{N_1N_2}) + O(\overrightarrow{N_1N_2}),$$
$$u(N_4) = u(N_1) + (\nabla u(N_1), \overrightarrow{N_1N_4}) + O(\overrightarrow{N_1N_4}).$$

Then

$$\nabla u(N_1) = B^* \begin{bmatrix} u_1 \\ u_2 \\ u_3 \\ u_4 \end{bmatrix} + \max_{i \neq j}(O(\overrightarrow{N_iN_j})) \tag{8}$$

with

$$B^* = \frac{1}{\Delta^*} \begin{bmatrix} y_2 - y_4 & y_4 - y_1 & 0 & y_1 - y_2 \\ x_4 - x_2 & x_1 - x_4 & 0 & x_2 - x_1 \end{bmatrix}$$

and

$$\Delta^* = (x_2 - x_1)(y_4 - y_1) - (x_4 - x_1)(y_2 - y_1).$$

With these two finite difference approximation schemes, 2 different integration scheme to compute the 'stiffness' matrix K follow : one node integration with (7), four nodes integration with (8). In this paper, we shall exclusively focus on the central finite difference approximation (7).

With the central finite difference approximation (7), on each quadrangular element E_k, the elementary 'stiffness' matrix simply reads :

$$K_{el} = B' * B|E_k|.$$

where $|E_k|$ is the measure of the element.

Numerical results on the scalar model problem (1)

We apply the finite difference method to the Poisson problem (3) with $\Omega = [-\frac{1}{2}, \frac{1}{2}]^2$. Due to the symmetries of the problem we compute on a quarter of the domain only, that is $[0, \frac{1}{2}]^2$. With a set of regular and distorted $k \times k$ meshes where the parameter k denotes the number of subdivision of the domain, see Figure 2.

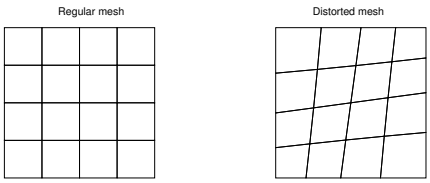

Figure 2: Regular and distorted 4x4 meshes

We consider the finite difference element procedure with one degree of freedom (DOF) per node, for which we solely use the (7) central finite difference approximation coupled with one node integration scheme; we call this element FDEM4.

In Figure 3, we display the relative error of the solution at the center of Ω, where it takes its maximal value, compared to the exact solution (obtained through Fourier series) and the computed solution by a standard four node quadrangle polynomial element, QUA4.

We can see that FDEM4 element converges with an apparent nearly quadratic rate, even though it is clearly outperformed by QUA4. The convergence rate for FDEM4 does not show much sensitivity to mesh distorsion, whereas it deteriorates for QUA4 in the case of distorted meshes. This is not surprising since the finite difference scheme (7) is independent of the shape of the quadrangular and the P2 polynomial interpolation of QUA4 is incomplete. These numerical results already indicate the behavior of FDEM4 element : it will have average to poor performance on very coarse meshes, but the convergence rate should be nearly quadratic and should not be too sensitive on mesh distorsion.

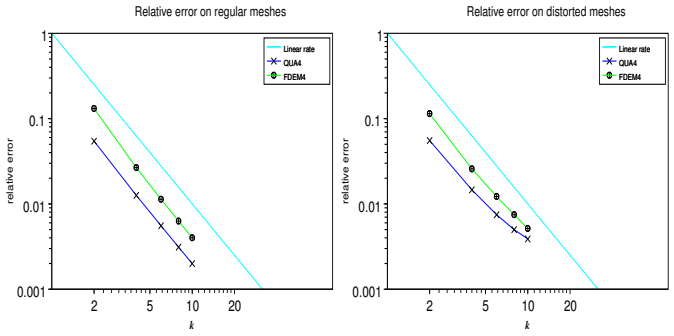

Figure 3: Relative error $\frac{u_h - u}{u}$ at $(0, 0)$ for regular and distorted $k \times k$ meshes.

Galerkin or not ?

Our interpretation of the Finite Difference Element Method, is that the rough integration scheme can nevertheless be exact for some class of shape functions. From this point of view, the Finite Difference Element Method is even a conformal finite element method. A description of such a class is still under investigation, but we can reasonably conjecture such class is not void in the space of admissible solutions, in this case.

3. Thin elastic shells : the Naghdi's model

We refer to [6, 11] for a full description and presentation of the theory on thin shells in the Naghdi's model. We only recall the mechanical problem in static linear elasticity for a homogeneous and isotropic shell with Young's modulus E and coefficient of Poisson ν.

Let's first define a shell with its geometry, see Figure 4. Let S be the middle surface defined with the map $(\Omega, \overrightarrow{r}) : \Omega \in \mathbb{R}^2$ and

$$\overrightarrow{r} = x(x_1, x_2)\overrightarrow{e}_1 + y(x_1, x_2)\overrightarrow{e}_2 + z(x_1, x_2)\overrightarrow{e}_3. \tag{9}$$

The surface map defines the tangent vectors

$$\overrightarrow{a}_\alpha = \overrightarrow{r}_{,\alpha},$$

and the unit normal vector

$$\overrightarrow{a}_3 = \frac{\overrightarrow{a}_1 \wedge \overrightarrow{a}_2}{||\overrightarrow{a}_1 \wedge \overrightarrow{a}_2||}.$$

the three vectors $\overrightarrow{a}_i$ constitute the *covariant* basis of S. We keep in mind that the covariant basis is not a priori orthonormal nor orthogonal, we thus define the dual *contravariant* basis $\overrightarrow{a}^i$ in order to make scalar products.

Let ε be the constant thickness the shell, then any of its point can be given by the position vector, $\forall (x_1, x_2) \in \Omega$, $x_3 \in [-\frac{\varepsilon}{2}, \frac{\varepsilon}{2}]$,

$$\overrightarrow{p}(x_1, x_2, x_3) = \overrightarrow{r}(x_1, x_2) + x_3 \overrightarrow{a}_3.$$

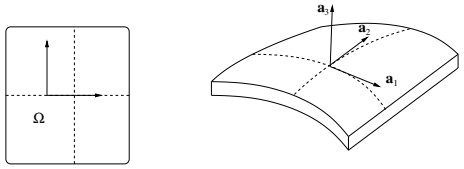

Figure 4: A Shell, the covariant basis of its midsurfcace

The Naghdi's model involves the displacement $\overrightarrow{u}$ and the rotation $\overrightarrow{\theta}$ to define the deformation of the shell under external loadings. Although the theory involves covariant components, we shall represent the displacement with its Cartesian component :

$$\overrightarrow{u} = u_i \overrightarrow{e_i}.$$

The rotation is tangent to S and thus can conveniently be represented by its covariant components:

$$\overrightarrow{\theta} = \theta_\alpha \overrightarrow{a}^\alpha.$$

Under external loadings, represented by a linear form L^ε, we define the mechanical problem of thin elastic shells in its variational form as follows, where V denotes a Sobolev space of kinematically admissible displacements and rotations :

$$\begin{cases} \text{Find } U = (\overrightarrow{u}, \overrightarrow{\theta}) \in V \text{ such that} \\ a_\varepsilon(U, U^*) = L^\varepsilon(U^*) \quad \forall U^* \in V. \end{cases} \tag{10}$$

The bilinear form of deformation energy, a_ε, for any $U = (\overrightarrow{u}, \overrightarrow{\theta})$ and $U^* = (\overrightarrow{u}^*, \overrightarrow{\theta}^*)$, is :

$$a_\varepsilon(U, U^*) = \varepsilon^3 a^b(U, U^*) + \varepsilon a^s(U, U^*) + \varepsilon a^m(U, U^*) \tag{11}$$

where the energy form is respectively decomposed in bending, shear and membrane parts :

$$a^b(U, U^*) = \int_\Omega \frac{1}{12} A^{\alpha\beta\lambda\mu} \rho_{\alpha\beta} \rho_{\lambda\mu} \tag{12}$$

$$a^s(U, U^*) = \int_\Omega C^{\alpha\beta} \Lambda_\alpha \Lambda_\beta \tag{13}$$

$$a^m(U, U^*) = \int_\Omega A^{\alpha\beta\lambda\mu} \gamma_{\alpha\beta} \gamma_{\lambda\mu} \tag{14}$$

where $\gamma_{\alpha\beta}$ and $\rho_{\alpha\beta}$ respectively represent the variation tensors of the first and second fundamental form of the surface S, measuring the variation of length and variation of curvature. The Λ_α measure the shear :

$$\gamma_{\alpha\beta} = \frac{1}{2}\left(\overrightarrow{u}_{,\alpha}.\overrightarrow{a}_\beta + \overrightarrow{u}_{,\beta}.\overrightarrow{a}_\alpha\right) \tag{15}$$

$$\rho_{\alpha\beta} = \frac{1}{2}\left(\overrightarrow{\theta}_{,\alpha}.\overrightarrow{a}_\beta + \overrightarrow{\theta}_{,\beta}.\overrightarrow{a}_\alpha - \overrightarrow{a}_{3,\alpha}.\overrightarrow{u}_{,\beta} - \overrightarrow{a}_{3,\beta}.\overrightarrow{u}_{,\alpha}\right) \tag{16}$$

$$\Lambda_\alpha = \theta_\alpha + \overrightarrow{u}_{,\alpha}.\overrightarrow{a}_3. \tag{17}$$

Since the shell is homogeneous and isotropic, the constitutive law is given by :

$$A^{\alpha\beta\lambda\mu} = \frac{E}{2(1+\nu)}\left[a^{\alpha\lambda}a^{\beta\mu} + a^{\alpha\mu}a^{\beta\lambda} + \frac{2\nu}{1-\nu}a^{\alpha\beta}a^{\lambda\mu}\right] \tag{18}$$

$$C^{\alpha\beta} = \frac{E}{4(1+\nu)}a^{\alpha\beta}. \tag{19}$$

with the contravariant components of the first fundamental form

$$a^{\alpha\beta} = \overrightarrow{a}^\alpha.\overrightarrow{a}^\beta.$$

Asymptotic behavior and Numerical difficulties

The natural trend for a very thin elastic shell is to perform bendings as, from (10), shear and membrane deformation energies are penalized when the thickness ε is very small, see also [27, 11, 26]. But, unlike the bendings in beams problems, bending deformation on a surface is not always admissible : it depends on the boundary conditions and the geometry [18]. Thin shells are thus classified as [with bendings] *inhibited* or *not-inhibited*, following the terminology introduced by Sanchez-Palencia[27].

This classification is also referred as *membrane dominated* and *bending dominated* [24, 17]. These two very distinct asymptotic behaviors lead to strong difficulties in the numerical approximation of very thin elastic shells by finite element procedures : boundary layers, propagation and reflexion of singularities, sensitivity within the inhibited case and numerical (membrane) locking in the non-inhibited or bending dominated case, see [24, 25, 16, 11, 20, 26].

Classically, we have the following asymptotic behavior valid for thin shells linear models such as Koiter's or Naghdi's [26, 17, 11]:

Theorem 1. *If the (scaled) load $L^\varepsilon(\overrightarrow{v})$ depends on ε as $L^\varepsilon(\overrightarrow{v}) = \varepsilon^3 L(\overrightarrow{v})$, then the solutions $\overrightarrow{u}^\varepsilon$ of* (10) *converge (weakly in $\overrightarrow{V}$) towards the solution $\overrightarrow{u}^0$ of the asymptotic (limit) bending problem*

$$\begin{cases} \textit{find } \overrightarrow{u}^0 \in \overrightarrow{G} \textit{ such that} \\ \displaystyle\int_S \frac{A^{\alpha\beta\lambda\mu}}{12}\rho_{\alpha\beta}(\overrightarrow{u}^0)\rho_{\lambda\mu}(\overrightarrow{v}), = L(\overrightarrow{v}^*), \quad \forall \overrightarrow{v}^* \in \overrightarrow{G}, \end{cases} \tag{20}$$

where $\overrightarrow{G}$ is the set of kinematically admissible infinitesimal bendings (also called inextensional displacement) :

$$\overrightarrow{G} = \left\{\overrightarrow{u} \in V \textit{ such that } \gamma_{\alpha\beta}(\overrightarrow{u}) = 0\right\}.$$

and where we replaced θ_α in $\rho_{\alpha\beta}$ with $-\overrightarrow{u}_{,\alpha}.\overrightarrow{a}_3$.

We recall that infinitesimal bendings are solutions of a partial differential equation, the nature of which depends on the nature of the surface. In particular, if a surface is defined by a position vector :

$$r(x_1, x_2) = x_1 \overrightarrow{e}_1 + x_3 \overrightarrow{e}_2 + \varphi(x_1, x_2) \overrightarrow{e}_3,$$

the vertical component u_3 of any infinitesimal bendings on the surface satisfies the second order PDE :

$$\varphi_{,22} u_{3,11} + 2\varphi_{,12} u_{3,12} + \varphi_{,11} u_{3,22} = 0, \tag{21}$$

the characteristics of which corresponds to the *asymptotic lines* of the surface [18]. Namely, the nature of equation (21) is respectively hyperbolic, parabolic, elliptic when the surface is hyperbolic, developpable, elliptic.

This essential property underlines the fundamental importance of the asymptotic lines and therefore the topology of a meshing when dealing with the membrane locking, see [1, 27, 11].

In the inhibited shell cases, that is, when the space of infinitesimal bendings $\overrightarrow{G}$ reduces to $\{0\}$ or rigid displacements, which is the most common situation in practice, the theorem 1 simply indicates that the solutions $\overrightarrow{u}^{\varepsilon}$ converge to 0, as $\varepsilon \searrow 0$.

To fully analyze the *membrane dominated* asymptotic behavior, we need to change the scale of the loading from $\varepsilon^3 L$ to $\varepsilon^{\alpha} L$ with $1 < \alpha < 3$, see [11, 20] depending on the case. We shall not recall here all the subtleties of membrane dominated case, we simply recall that singularities and boundary layers appear, which make accurate computations difficult :

Theorem 2. *With the loading scaled as $L^{\varepsilon} = \varepsilon L$, if the shell is inhibited, then as ε decreases towards 0, the solution $\overrightarrow{u}^{\varepsilon}$ of problem* (1) *converge weakly to $\overrightarrow{u}$ the solution of the membrane limit problem :*

$$\begin{cases} \text{find } \overrightarrow{u} \in \overline{V}^m \text{ such that} \\ \displaystyle\int_S A^{\alpha\beta\lambda\mu} \gamma_{\alpha\beta}(\overrightarrow{u}) \gamma_{\lambda\mu}(\overrightarrow{v}^*), = L(\overrightarrow{v}^*), \quad \forall \overrightarrow{v}^* \in \overline{V}^m, \end{cases} \tag{22}$$

for any $L \in \overline{V}^{m\prime}$,

where $\overline{V}^m$ is the completion of V for the norm associated with a^m. In some cases $\overline{V}^m$ may be so big that it is not contained in the space of distributions. The shell is then said *ill-inhibited*, see [26]. The corollary is that the dual space $\overline{V}^{m\prime}$ can be very small : a uniform loading may even not be admissible in most cases with a free edges. This explains the singularities and boundary layer appearing in the inhibited or membrane dominated shells or even the instabilities such as the *chancelling* shells [21]. The asymptotic behavior of inhibited (membrane dominated) shells thus may vary depending on the loading [26, 11].

4. The FDEM4 shell element

The FDEM4 shell element we propose here is based on the Naghdi's Shell Model presented in section 3. The element is simply defined as replacing all first order differentials, in equations (15-17), involved in the variational problem of Naghdi's shell (10) by the central finite difference scheme (7). The integration is then obtained through a single node integration at the intersection of the diagonals of each quadrangular element.

It is indeed a very simple element, very cheap from a computational point of view, since the elementary stiffness matrix is only evaluated once per element. We believe no shell element can possibly be more simple.

Each node have 5 degrees of freedom (DOF) : the 3 Cartesian components, u_i , of the displacement and 2 covariant components, θ_α, of the rotation. We remark from (16), that it is not necessary to compute the derivatives of the covariant component of the rotation, we simply need to compute the derivatives of the rotation by their expressions in the Cartesian basis, in order to apply the finite difference scheme (7). We make the computation directly on each element without dealing with a reference element.

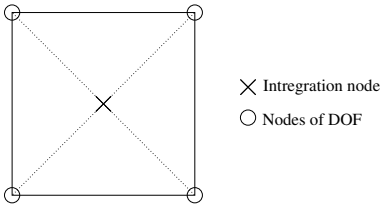

Figure 5: The FDEM4 shell element

In an algebraic way, such 'reduced' integration scheme reduces the number of constraints coming from shear and bendings condition : two conditions from the shear constraints and another three from the bending condition, when in bending dominated situations. Thus, a simple count of the number of available DOF, suggest that the FDEM4 to be locking free, or at least less sensitive to the locking effect.

Aside this (necessary) algebraic account, the finite difference element method procedure allows another interpretation : we conjecture there is a class of shape functions such that the finite difference element schemes coincide with the integral involved in (3), we *expect* then this class of functions to be large enough to 'contain' infinitesimal bendings. The existence and description of such a class certainly depends on the geometry and the mesh topology.

This work is preliminary, we chose to use exact geometry for the definition of the surface, that is, we use the exact expressions of the covariant basis and theirs derivatives. The development of FDEM shell procedure using only the coordinates of the nodes of the surface is in progress.

5. Numerical results

In this section, we follow [10, 24, 14, 15] to test the performance of the quadrangular finite difference element, FDEM4, on several cases of inhibited and non-inhibited shells and compare with widely used shell elements, namely the 3-nodes triangular plane facet Discrete Kirchhoff Triangle (DKT) shell ele-

ment within the CasT3M[1] software and the 4-nodes quadrangular MIxed Tensorial Components (MITC4) element within the software Scilab[2] and the package OpenFEM, [5, 3].

We used the same meshes for FDEM4 and MITC4, but for the triangular DKT element, we divided each quadrangle of the meshes in 4 triangular parts, thus our computations with DKT involve significantly more nodes and DOF than their quadrangular counterparts.

5.1. A plate as a plane shell

We start the numerical tests with the case of a plate, for which the Nagdhi's model reduces to Reissner-Mindlin plate model. The test is interesting from the numerical locking point of view because it first evaluates the robustness with respect to shear locking.

We consider the classical example of a circular plate clamped all along its boundary.It is submitted to an uniform vertical loading. To test the shear locking we have taken a very small thickness, $\varepsilon = 10^{-4}$ (tests with smaller thicknesses give nearly identical results). Taking advantage of the axial symmetries of the problem, the computational domain is reduced to a quarter of the domain, see figure 6.

In Figure 7, we plot the relative error on the central deflection, compared to exact analytical solution of the problem within Kirchhoff-Love plate model. We display the errors for various regular $k \times k$ mesh, k being the number of element subdivision of one side of the quarter of the domain. The size of the mesh being $h = \frac{1}{k}$.

The FDEM4 plate element is convergent with quadratic rate but is outperformed by both DKT and MITC elements. This is similar to the scalar model case. (1). Nevertheless, the shear locking is not present in FDEM4 for this test.

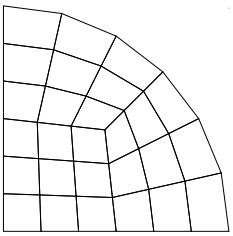

Figure 6: A quadrangular $k \times k$ mesh of the quarter of the circular plate with refinement parameter $k = 6$.

5.2. An inhibited cylindrical shell, the Scordelis-Lo roof

We start the numerical test on shells with a classic: the Scordelis-Lo roof. It is a cylindrical shell supported by rigid diaphragms at its end edges, the two other boundaries along the generatrices are free. The shell is submitted to a uniform vertical loading. Due to the plane symmetries of the problem, the

[1]Cast3M is available at `http://www-cast3m.cea.fr` and is developed by the Commissariat à l'Énérgie Atomique.

[2]Scilab is available at `http://www.scilab.org` and is developed by the INRIA.

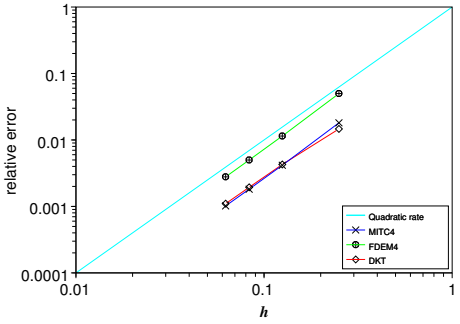

Figure 7: Circular clamped plate. The relative error of central displacement $\frac{u_{exact}-u}{u_{exact}}$ compared to the exact solution.

computed domain is reduced to one forth of the cylinder, see Figure 8.The original benchmark proposed takes a fixed relative thickness $\varepsilon = \frac{3}{300} = 10^{-2}$, the Young's modulus $E = 3.10^6$, the Poisson coefficient $\nu = 0$ and the vertical load $L = 0.625$, the coherent units being inches and pounds.

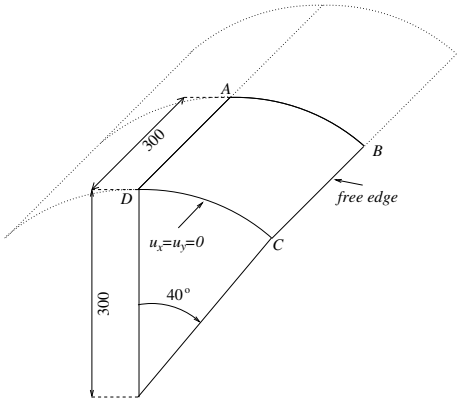

Figure 8: Scordelis-Lo roof

We plot the value of the vertical component at midside B normalized by a reference value and for $k \times k$ regular meshes, see Figure 9. The reference values are the exact analytical solution based on Flugge's shell theory, see [8], and are given in Table 1. We note that the FDEM4 seems to converge but is slightly overestimating the deflection, unlike to DKT and MITC4.

We push forward this example by decreasing the relative thicknesses from $\varepsilon = 10^{-2}$ to 10^{-5}. We refer to [6, 11] for a complete asymptotic analysis of the test, but we emphasize on the fact it is a case of inhibited shell, more precisely *ill-inhibited* shell. The vertical loading does not belong to the space $\overline{V}^{m\prime}$ and thus is not admissible : boundary layers appear along the free edges if the thickness is chosen very small. The width of this boundary layer was shown, in [19], to be proportional to $\varepsilon^{\frac{1}{4}}$. We then take account of this information, choosing $\frac{3}{2}\varepsilon^{\frac{1}{4}}$ as the width of the boundary layer to define adapted meshes equally refined inside and outside the boundary layer, see Figure 10. This can be seen as a test on whether the FDEM4 is suitable for

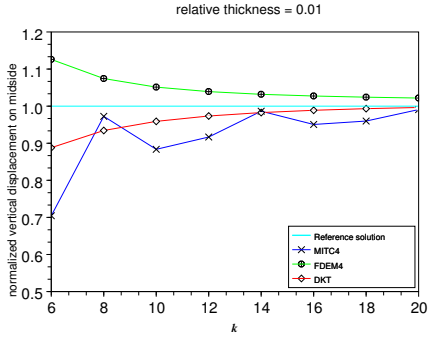

Figure 9: Vertical deflection on midside of Scordelis-Lo roof for regular $k \times k$ meshes, normalized by a reference solution.

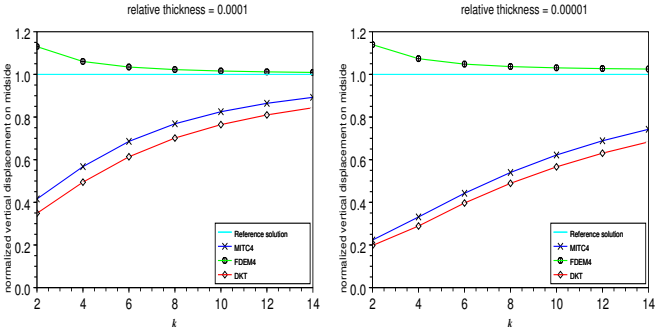

Figure 11: Normalized deflection on midside on Scordelis-Lo roof with adapted $(k + k) \times k$ meshes.

adapted meshes with stretched elements. We scaled the loading by a $\frac{\varepsilon^2}{9}$ factor. In Figure 11 we plot the deflection on midside of the free edge normalized by a reference value, see Table 1. The FDEM4 performs here very well with a satisfactory convergence rate, and clearly better than both DKT and MITC4 when the relative thickness $\varepsilon = 10^{-4}$ or $\varepsilon = 10^{-5}$.

ε	10^{-2}	10^{-3}	10^{-4}	10^{-5}
$\tilde{u}_3$	3.6285	3.9528	4.0882	4.0805

Table 1: Reference value of vertical deflection on midside of Scordelis-Lo roof for relative thickness from 10^{-2} to 10^{-5}, based on Flugge's shell theory.

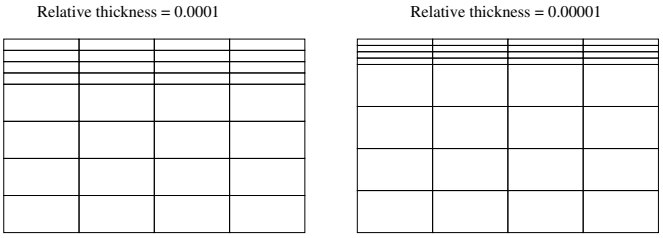

Figure 10: Adapted $(k + k) \times k$ meshes with $k = 4$.

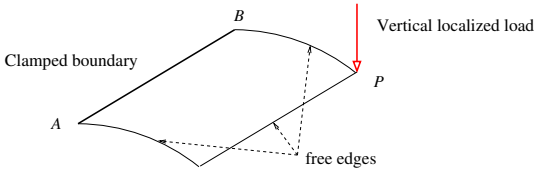

Figure 12: A Cylinder clamped along AB and subjected to a vertical load localized on P.

5.3. *A partially clamped non inhibited cylindrical shell*

We continue with a cylindrical shell, but choose the boundary conditions so that the infinitesimal bendings are rendered admissible. We roughly take a simplified Scordelis-Lo cylinder partially clamped along a generatrice (straight edge) while the other edges are free. We impose a localized loading on a free corner as shown in Figure 12. The geometry is defined by :

$$x = x_1, \quad y = x_2, \quad z = \varphi(x), \quad \forall (x_1, x_2) \in \Omega, \qquad (23)$$

with $\varphi(x_1) = \sqrt{1 - x_1^2}$ and $\Omega = [0, \frac{\sqrt{2}}{2}] \times [-0.5, 0.5]$. The shell is subjected to a vertical force $\overrightarrow{F^\varepsilon} = \varepsilon^3 \overrightarrow{e}_3$ *localized* at the point $P = (\frac{\sqrt{2}}{2}, 0.5, \frac{\sqrt{2}}{2})$; note the ε^3 scaling corresponding to a non-inhibited shell.

This test is not classical, we preferred it over the full cylinder with free ends and subjected to a periodic pressure, see for instance [10]. The main reason is the more complex shape of the solution in our test; the test becomes henceforth 'tougher' than the full cylinder one. To our best knowledge, no analytic solution for this problem is available but it is possible to solve the associated asymptotic bending problem (20) [15]. The asymptotic solution can then be used as a reference as the thickness we is decreased .

Equation (21) which characterizes the vertical component of an infinitesimal bending reduces then to

$$\varphi_{22} u_{3,11} = 0.$$

The vertical component of an infinitesimal bending on the cylinder are then the polynomials in x_2 with arbitrary functions g and h of the variable x_1 :

$$u_3 = g(x_1) + x_2 h(x_1).$$

The shell being now clamped along the straight line $x_1 = 0$, all vertical displacements $u_3 = g(x_1) + x_2 h(x_1)$ satisfying the boundary conditions $g(0) = g'(0) = h(0) = h'(0) = 0$, define admissible infinitesimal bendings. The shell is thus non-inhibited.

The bending limit problem (20) reduces then to a one dimensional differential problem :

Proposition 3. *The vertical component u_3^0 of the asymptotic bending problem* (20) *can be computed by solving a variational*

problem of two functions of one variable :

$$\begin{cases} \text{Find } u_3^0 = g(x_1) + x_2 h(x_1) \in V \\ \displaystyle\int_S \frac{1}{12}\left[A^{1111}\rho_{11}\rho_{11}^* + 4A^{1212}\rho_{12}\rho_{12}^*\right] = L(u_3^*), \\ \forall u_3^* = g^*(x_1) + x_2 h^*(x_1) \in V. \end{cases} \tag{24}$$

We don't have the exact analytical solution of the reduced asymptotic bending problem (24), but it can be solved using standard one dimensional finite element procedure. To fix the idea, the value of the vertical displacement at P is set to $u_3^0 = 2.1168107$, for $E = 1$, $\nu = 1/3$ and unitary vertical load.

We note that in this case, the vertical displacement on P of the limit bending solution equals to the limit flexion energy or the asymptotic energy :

$$u_3^0(P) = a^b(\overrightarrow{u}^0, \overrightarrow{u}^0).$$

From minimizing energy results, we remind that if u^ε is the solution of (10) with the scaled loading L^ε then, we have necessarily :

$$u_3^0(P) \leq u_3^\varepsilon(P) \quad \forall \varepsilon > 0.$$

The value of the vertical component at P is then a good criteria as to evaluate a finite element computation in this case. convergence for regular and distorted meshes are shown in Figure 13, where the distorsion is defined as a geometric sequence of common ratio 1.1. We must keep in mind that with such distorted meshes, the asymptotic lines are no more represented by some sides of the elements. To test the membrane locking, we run computations for thicknesses from 10^{-2} to 10^{-4}.

Figure 13: Regular and distorted $k \times k$ meshes, with $k = 4$.

In the Figure 14, we plot the vertical displacement normalized by the solution of the asymptotic (bending) limit problem (24) using $k \times k$ regular meshes for various values of k, the number of subdivisions of the interval $[0, \frac{\sqrt{2}}{2}]$ For the thickness $\varepsilon = 10^{-2}$ we see that DKT, MITC4 and FDEM4 are coherent and converge to the same solution. As the thickness decreases, we clearly see that DKT underestimates the real solution whereas the MITC4 and FDEM4 are both coherent with the asymptotic analysis and seem to converge. In this case, the membrane locking is absent for both MITC4 and FDEM4 whereas present with DKT.

In the Figure 15, we plot the vertical displacement normalized by a reference solution using quasi uniform distorted $k \times k$ meshes, see Figure 13 , for various values of mesh refinement parameter k. As a reference solution, we used the value obtained with MITC4 element with a 28x28 regular mesh. We

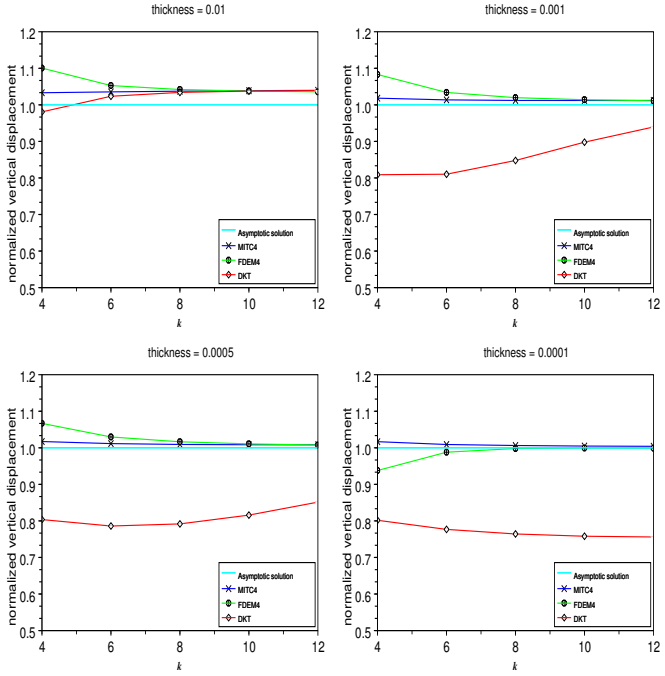

Figure 14: Non-inhibited partially clamped cylinder submitted to vertical localized load, with regular meshes, $\frac{u_3^\varepsilon(P)}{u_3^0(P)}u$ for thicknesses from 10^{-2} to 10^{-4}.

note in this case that the reference solution is not very different from the asymptotic solution.

The locking is still present for DKT. On the contrary MITC4 shows signs of significant deterioration of the approximation for very small thicknesses ($\varepsilon = 5.10^{-4}$), while FDEM4 seems unaffected.

5.4. A partially clamped non-inhibited hyperbolic paraboloid

We study here the case of a partially clamped hyperbolic paraboloid defined for any $(x_1, x_2) \in \Omega = \left[-\frac{\sqrt{2}}{2}, \frac{\sqrt{2}}{2}\right]^2$

$$x = x_1, \quad y = x_2, \quad z = \frac{1}{2}(x_1^2 - x_2^2). \tag{25}$$

Note that the last surface is equivalently defined by

$$x = x_1, \quad y = x_2, \quad z = x_1 x_2, \quad \forall (x_1, x_2) \in \Omega_l \tag{26}$$

where Ω_l is the quadrangle defined by the four points $A : (-1, 0)$, $B : (0, -1)$, $C : (1, 0)$, $D : (0, 1)$, see figure 16

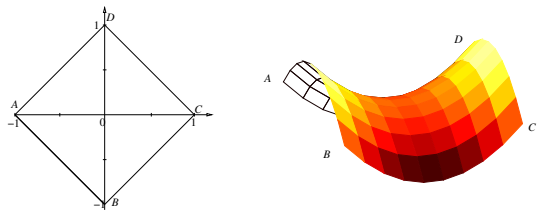

Figure 16: A hyperbolic paraboloid, partially clamped, along AB, and submitted to uniform vertical load.

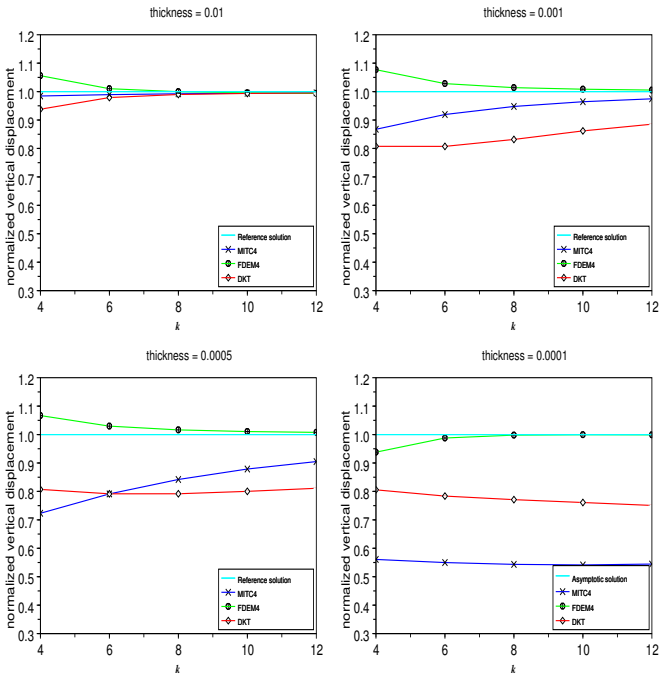

Figure 15: Non-inhibited partially clamped cylinder submitted to vertical localized load, with distorted meshes, $\frac{u_3^\varepsilon(P)}{u_3^0(P)}u$ for thicknesses from 10^{-2} to 10^{-4}

Here again we compare FDEM4 with MITC4 and DKT with respect to the solution of the bending limit problem. In the case of hyperbolic paraboloid defined by the map (26), equation (21) characterizing the vertical component of an infinitesimal bending reduces to

$$\varphi_{,12}u_{3,12} = 0.$$

Then any arbitrary functions f and g of one variable define the vertical components of any inextensional displacements (or infinitesimal bendings) on the paraboloid :

$$u_3(x_1, x_2) = g(x_1) + h(x_2) \quad \forall (x_1, x_2) \in \Omega_l$$

We recall that when the shell is clamped along the AB boundary, it is not inhibited although bendings necessarily vanishes in the subdomain $\{(x_1, x_2) \in \Omega / \quad x_1 \leq 0 \text{ and } x_2 \leq 0\}$. It suffices then that g and h and their derivatives vanishes on $[-1, 0]$ and be arbitrary on $]0, 1]$.

On such shell problem, the limit bending limit problem can be reduced to a more simple formulation, see [14] :

$$\begin{cases} \text{Find } u_3 = g(x_1) + h(x_2)/g, h \in V^2 \\ \frac{1}{12}\int_{\Omega_l} \begin{bmatrix} g'' \\ h'' \end{bmatrix}^\top \begin{bmatrix} A^{1111} & A^{1122} \\ A^{2211} & A^{1222} \end{bmatrix} \begin{bmatrix} g^{*\prime\prime} \\ h^{*\prime\prime} \end{bmatrix} a^{\frac{3}{2}} \\ = \quad \int_{\Omega_l} (g^*(x_1) + h^*(x_2)) a^{\frac{1}{2}}, \\ \quad \forall g^*, h^* \in V^2 \end{cases} \tag{27}$$

where

$$V = \{f \in \mathbb{H}^2([0, 1])/f(0) = f'(0) = 0\}.$$

In Figure, 18 and 19, we normalized the vertical displacement on corner node D by the solution of the bending limit problem. We used regular and distorted meshes, see Figure 17, for various values of mesh refinement parameter k. The mesh distorsion is again defined as geometric sequence of common ratio 1.1.

As we can see no membrane locking arises on regular meshes and the results are consistent with the asymptotic behavior, we observe that the computed solutions converge to the asymptotic bending limit solution as the thickness decreases towards zero. The convergence rate seems good but FDEM4 is underperforming compared to both DTK and MITC4.

Figure 17: regular and distorted $k \times k$ meshes, with $k = 6$.

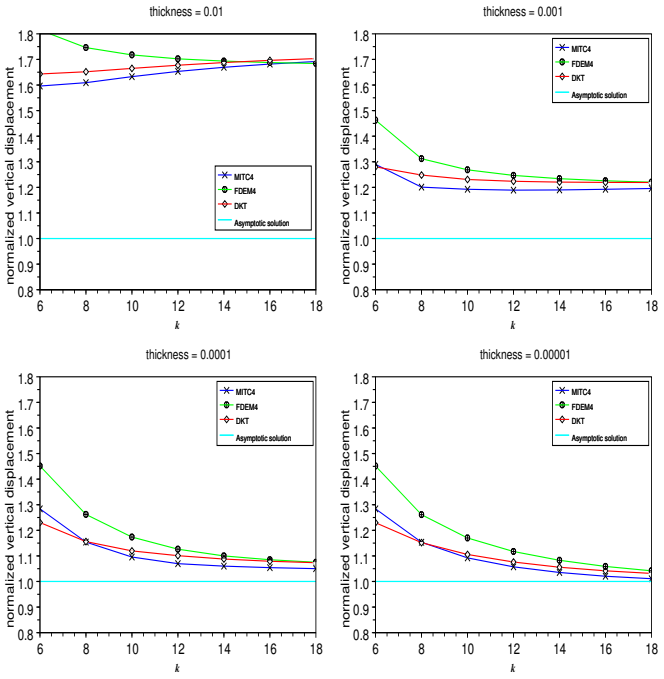

Figure 18: Non-inhibited partially clamped hyperbolic paraboloid. Normalized vertical displacement on $k \times k$ regular meshes

In Figure 19, we plot the computed normalized vertical component on corner node D for distorted $k \times k$ meshes. The vertical displacement is normalized with by a reference solution obtained with the MITC4 solution and a very thin regular mesh (28x28), see table 2, except for the smallest thickness $\varepsilon = 10^{-5}$ for which we normalized by the asymptotic solution.

It appears that the computations from both DKT and MITC4 presents severe signs of deterioration for thicknesses below 10^{-3}.

FDEM4 also presents slight signs of computational deterioration but in a very different magnitude and overall correct except for the smallest thickness for which the error in vertical deflection is nearly 20%.

ε	10^{-2}	10^{-3}	10^{-4}	Asymp. solution
$\tilde{u}_3$	0.86	0.60580	0.52349	0.5006

Table 2: Reference value of vertical deflection at D compared to the asymptotic solution.

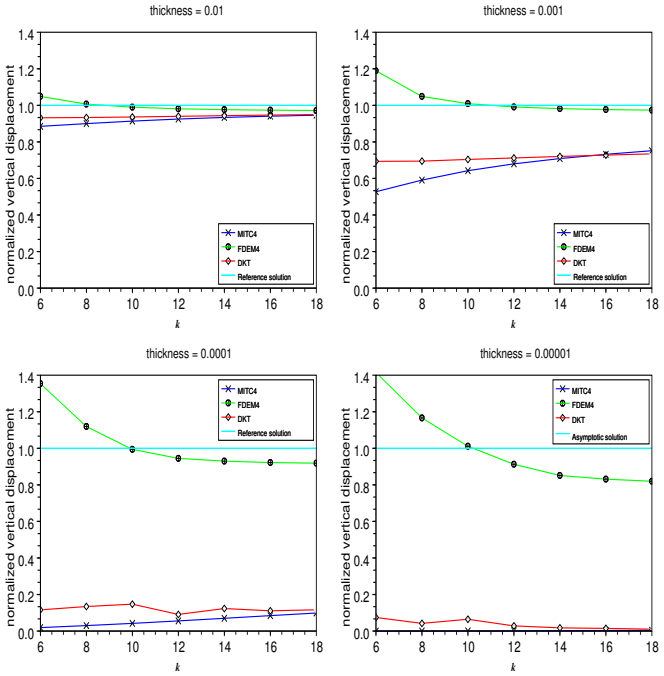

Figure 19: Non-inhibited partially clamped hyperbolic paraboloid. Normalized vertical displacement on $k \times k$ distorted meshes

5.5. A clamped inhibited hyperbolic paraboloid

We consider again the geometry of section 5.4 and uniform vertical loading but the shell is now clamped all along its boundary, the shell is with bendings inhibited.

Instead of focusing on the deflection on one particular point, we had rather study the convergence in energy norms. In Figure, we plot the relative errors from computations on regular $k \times k$ meshes with respect to the values obtained with a 60×60 mesh.

In Figure 20, the convergence rate seems almost quadratic again. For very small thicknesses ($\varepsilon < 10^{-3}$), we detect instabilities, illustrated by the poor convergence of the bending and shear energy, that disappear with finer meshes. Although, we didn't detect spurious modes, we think the existence of *pseudo-bendings* [28, 13], explains the instabilities. Note that those instabilities are also present for DKT and MITC4.

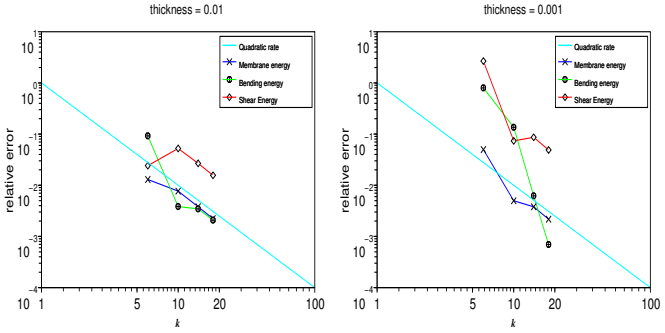

Figure 20: Non-inhibited clamped hyperbolic paraboloid. Relative errors of membrane, flexion, total energy on $k \times k$ regular meshes

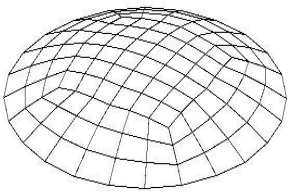

Figure 21: Spherical cap with 6×6 quadrangular mesh.

5.6. A clamped well-inhibited spherical cap

We consider her the spherical cap defined with the position vector, $\forall (x_1, x_2) \in \Omega$

$$r(x_1, x_2) = \sqrt{4 - x_1^2 - x_2^2}$$

where $\Omega = \{(x_1, x_2) \in \mathbb{R}^2 / x_1^2 + x_2^2 \leq 1\}$, see Figure 21. The geometric nature is elliptic, there are no asymptotic lines in that case. The shell is clamped all along it boundary, the shell is then inhibited, more precisely well-inhibited and the completed space $\overline{V}^m$ is included in $H_0^1 \times H_0^1 \times \mathbb{L}^2(\Omega)$ (for tangent and normal components of the displacement), see [26].

We impose a uniform vertical load. As the problem is invariant by axial rotation, we use the computed solution of an axisymmetric shell element as reference. We plot, in Figure 22, the relative error of the vertical displacement at the top the spherical cap. In this case, DKT, MITC4 and FDEM4 all present instabilities, although less important for MITC4. While we observe convergence, the instabilities grows as the thickness decreases for a fixed mesh. For FDEM4, it is due to the existence, in this elliptic case, of a spurious mode for the asymptotic membrane problem (22) that is stabilized by the bending energy.

6. Conclusions and perspectives

We have proposed an original four node quadrangular shell finite element, FDEM4, using a finite difference element method procedure based on the quest of a Galerkin method without explicit shape functions. The FDEM4 shell element derives directly from the Naghdi's shell model without any corrections.

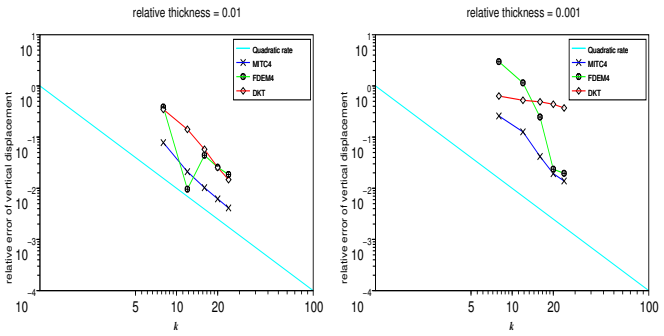

Figure 22: Well-inhibited clamped spherical cap with uniform loading. Normalized vertical displacement at (0,0).

The element is simple and cost effective due one node integration scheme in the construction of the stiffness matrix.

The numerical tests on plates, inhibited and non-inhibited shells, with regular and distorted meshes are very encouraging : the FDEM4 has constantly showed convergence behavior with almost quadratic rate in every cases we have tested. In most cases, FDEM4 also compares favorably to MITC4 or DKT.

In non-inhibited cases, the computed solutions are compared with the solution of the asymptotic bending problem. As the thickness is decreased, we observe a coherent asymptotic behavior of FDEM4 with the asymptotic theory of thin shells.

In the case of a spherical cap (elliptic shell), the spurious mode for the membrane energy, even though stabilized by the bending energy, prevents FDEM4 to be an ideal quadrangular shell element. It also means that the Galerkin interpretation of the FDEM4 element presented here, fails at least for this geometry.

Overall, the constant convergence behavior, the good robustness to distorsion and membrane locking makes the FDEM4 an interesting and already mostly reliable shell element. It offers a perspective for more robust and perhaps more performant shell elements based on this concept. We may for example adapt the finite difference scheme with respect to the geometric nature of the shell.

Much work still need to be done apart from improving robustness : a theoretical study of convergence and the interpretation of finite difference element method as part of the Galerkin method's family. We need also to develop facet based FDEM element instead of an exact definition of the geometry. Of course, one of the most important, of utmost engineering interest, is the development of triangular shell elements, as quadrangular discretisation cannot always be easily available.

References

[1] J.-L. Akian and E. Sanchez-Palencia. Approximation de coques élastiques minces par facettes planes. phénomènes de blocage membranaire. *C. R. Acad. Sci. Série I*, 315:363–369, 1992.

[2] D. N. Arnold and F. Brezzi. Locking free finite element methods for shell problem. *Mathematics of Computation*, 66(217):1–14, 1997.

[3] K.-J. Bathe. *Finite Element Procedures*. Prentice Hall, 1996.

[4] K.-J. Bathe, A. Iosilevich, and D. Chapelle. An evaluation of the mitc shell elements. *Computers & Structures*, 75(1):1 – 30, 2000.

[5] J. L. Batoz and P. Lardeur. A discrete shear triangular nine d.o.f. element for the analysis of thick to very thin plates. *International Journal for Numerical Methods in Engineering*, 1989.

[6] M. Bernadou. *Méthodes d'éléments finis pour les problèmes de coques minces*. Masson, Paris, 1994.

[7] K.-U. Bletzinger, M. Bischoff, and E. Ramm. A unified approach for shear-locking-free triangular and rectangular shell finite element. *Computers & Structures*, 75:521–534, 2000.

[8] D. Briassoulis. Asymptotic deformation modes of benchmark problems suitable for evaluating shell elements. *Computer Methods in Applied Mechanics and Engineering*, 194(21-24):2385 – 2405, 2005. Computational Methods for Shells.

[9] D. Bushnell. Finite difference energy methods. *Computer and Structures*, 1971.

[10] D. Chapelle and K. J. Bathe. Fundamental considerations for the finite element analysis of shell structures. *Computers & Structures*, 66(1):19–36, 1998.

[11] D. Chapelle and K.-J. Bathe. *The finite element analysis of shells – Fundamentals*. computational fluid and solid mechanics. Springer, 2003.

[12] C. Chinosi and G. Sacchi. Numerical approximation of bending dominated shells using p.r.s.i schemes.

[13] D. Choï. On geometrical rigidity of surfaces. application to the theory of thin elastic shells. *Mathematical Models and Methods in Applied Science*, 7(4)(2):507–555, 1997.

[14] D. Choï. Computations on thin non-inhibited hyperbolic elastic shells. benchmarks for membrane locking. *Journal Mathematical Methods Aplie Sciences*, 22(15):1293–1321, 1999.

[15] D. Choï. Some solutions to the asymptotic bending problem of non-inhibited shells. *Third MIT Conference*, 2005.

[16] D. Choï, F. J. Palma, E. Sanchez-Palencia, and M. A. Vilariño. Remarks on membrane locking in the finite element computation of very thin elastic shells. *Modélisation Mathématique et Analyse Numérique*, 32(2):131–152, 1998.

[17] P. G. Ciarlet. *Mathematical Elasticity Volume III : Theory of shells*. Studies in Mathematics and its Applications. North Holland, 2000.

[18] G. Darboux. *Théorie générale des surfaces*, volume 4. Gauthier-Villars, 1896.

[19] P. Karamian, J. Sanchez-Hubert, and E. S. Palencia. A model problem for boundary layers of thin elastic shells. *M2AN*, 34(1), 2000.

[20] P. Karamian, J. Sanchez-Hubert, and E. S. Palencia. Non-smoothness in the asymptotics of thin shells and propagation of singularities. hyperbolic case. *International Journal of Mathematical Computational Science*, 22(1):81–90, 2002.

[21] J.-L. Lions and E. Sanchez-Palencia. Sensitivity of certain constrained systems and application to shell theory. *Journal de Mathématiques Pures et Appliquées*, 79(8):821–838, 2000.

[22] N. Nguyen-Thanh, T. Rabczuk, H. Nguyen-Xuan, and S. P. Bordas. A smoothed finite element method for shell analysis. *Computer Methods in Applied Mechanics and Engineering*, 198(2):165 – 177, 2008.

[23] V. Pavlin and N. Perrone. Finite difference energy technique for arbitrary meshes applied to linear plate problems. *International Journal for numerical methods in enginring*, 14:647–664, 1979.

[24] J. Pitkaranta. The problem of membrane locking in finite elements analysis of cylindrical shells. *Numerische Mathematik*, 61:523–542, 1992.

[25] J. Pitkaranta, Y. Leino, O. Ovaskainen, and J. Piila. Shell deformation states and the finite element method: A benchmark study of cylindrical shells. *computer methods in applied mechanics and engineering*, 128:81–121, 1995.

[26] J. Sanchez-Hubert and E. Sanchez-Palencia. *Coques élastiques minces : Propriétés asymptotiques*. Masson, 1997.

[27] E. Sanchez-Palencia. Statique et dynamique des coques minces, I et II. *C. R. Acad. Sci. Paris série I*, pages 411–417 et 531–537, 1989.

[28] I. N. Vekua. *Generalized analytic functions*. Pergamon Press, 1959. English translation.

[29] O. Zienkiewicz and R. Taylor. *The finite element method*. Butterworth Heinemann, fifth edition, 2000.